Water Resources and Industry 15 (2016) 1–13

Contents lists available at ScienceDirect

Water Resources and Industry

journal homepage: www.elsevier.com/locate/wri

Removal of methylene blue and mechanism on magnetic γ-Fe_2O_3/SiO_2 nanocomposite from aqueous solution

Dong Chen [a], Ziyang Zeng [b], Yubin Zeng [a,*], Fan Zhang [a], Mian Wang [a]

[a] Department of Water Quality Engineering, School of Power and Mechanical Engineering, Wuhan University, Wuhan 430072, China
[b] Department of Chemical Engineering & Applied Chemistry, University of Toronto, Toronto M5S 3E5, Canada

ARTICLE INFO

Article history:
Received 3 February 2016
Received in revised form
21 May 2016
Accepted 25 May 2016

Keywords:
Magnetic γ-Fe_2O_3/SiO_2
Methylene blue
Adsorption
Kinetics
Regeneration

ABSTRACT

Magnetic γ-Fe_2O_3/SiO_2 (M-γFS) nanocomposite was prepared using γ-Fe_2O_3 as the magnetic carriers. M-γFS was characterized by transmission electron microscope (TEM), X-ray diffraction (XRD), and Fourier Transform infrared spectroscopy (FTIR). The characterizations of M-γFS exhibit the irregular core-shell structure, and SiO_2 has been successfully coated on the surface of γ-Fe_2O_3. M-γFS has much higher adsorption capacity 116.09 mg/g calculated by coated SiO_2 on M-γFS than γ-Fe_2O_3 and SiO_2, and the alkaline conditions are beneficial to the adsorption of MB. Coexisting cations, ionic strength and humic acid can influence the adsorption capacity. Meanwhile, adsorption kinetics data for M-γFS show good fit to the pseudo-second-order kinetics model, and the Langmuir equation is more appropriate to describe the adsorption behavior of MB on M-γFS. Moreover, after recycling four times, M-γFS washed by ethanol can still keep high adsorption capacity for MB adsorption.

1. Introduction

Various dyes have been used in the production processes of the textile, printing and dyeing, and papermaking industries [1,2]. A large amount of these dyes have entered water bodies and become a threat to the water environmental safety. The dyes in the effluents, even at low concentrations, produce a number of toxic products via oxidation, hydrolysis and other chemical reactions [3], which either directly or indirectly cause harm to human health, e.g., by increasing the incidence of allergies, tumors and cancers [4]. Therefore, it is necessary to find simple, highly efficient, and economical methods to treat dye wastewater.

Currently, the methods of removal of dye including adsorption [5,6], membrane treatments, advanced oxidation processes [7–11], and biological treatments [12] have been studied extensively. Among these methods proposed, due to the high efficiency, cost effectiveness, and simple operation, the adsorption method has received an increasing attention [13,14]. The unique feature of the adsorption method is that no other reagent is required to promote the reaction rate between the adsorbent and adsorbate. Additionally, adsorbents generally have large specific surface areas and high removal of dye. Therefore, the adsorption to remove dyes from wastewater displays a number of advantages, such as rapid action and strong adaptability [15].

Traditional adsorbents, such as activated carbon, clay, silica, zeolites and other porous materials, have been investigated

* Corresponding author.
E-mail address: zengyubin@whu.edu.cn (Y. Zeng).

http://dx.doi.org/10.1016/j.wri.2016.05.003

widely [16–18]. Especially activated carbon is frequently used since it is effective for the removal of dissolved organic matter. Monika Wawrzkiewicz et al. used mixed silica-alumina oxide consisting of 4% SiO_2 and 96% Al_2O_3 to adsorb acid, reactive and direct dyes from aqueous solutions and from wastewater and got satisfactory results [19]. Dong Wei et al. reported an aerobic granular sludge as a biosorbent to treat dye wastewater, and achieved 80.72% removal of MB [20]. New sorbent rhamnolipid-functionalized graphene oxide (RL-GO) hybrid was prepared by one-step ultra-sonication and obtained a high adsorption capacity of MB onto RL-GO [21]. Nevertheless, the powder and gel adsorbents are difficult to separate from water except through high speed centrifugation; accordingly limiting their applicability. On the other hand, the powder and gel adsorbents cannot meet the developing industrial demands because of limited adsorption capacity and tedious recovery process. Additionally, difficulties in regenerating and high processing cost limit its applications [22]. Therefore, it is a challenge to develop materials with high adsorption capacity, good chemical stability and easy solid-liquid separation for the treatment of MB wastewater.

Magnetic field assisted separation technologies have a potential to provide new opportunities. Magnetic separation based on the superparamagnetic Fe_2O_3 has received high attention and has been widely used in wastewater treatment due to its convenience, economy and efficiency [23,24]. Hence, the aim of our study is to focus on the combination of magnetic particles γ-Fe_2O_3 and SiO_2 to overcome the disadvantage of traditional sorbents mentioned above. Based on this purpose, we prepared magnetic composites γ-Fe_2O_3/SiO_2 (M-γFS) which can not only be separated easily from liquid phase, but also possess a couple of advantages, such as high specific surface area, high adsorption capacity, strong paramagnetism, and stability in water without waste products. Moreover, M-γFS was characterized using TEM, XRD, FTIR, BET specific surface area, pore size distribution and magnetic saturation intensity. The adsorption capacity for dye MB on M-γFS and its mechanism including the influences of the initial solution pH, kinetics and adsorption isotherms were investigated. Meanwhile, regeneration of M-γFS was also evaluated in this study.

2. Materials and methods

2.1. Reagents and materials

All of the chemicals used were analytical grade except as noted. 2,4-DCP, tetraethyl orthosilicate (TEOS), anhydrous alcohol, methylene blue, ammonia, γ-Fe_2O_3 were analytical grade, all was purchased from SigmaeAldrich, USA. All solutions were prepared using deionized water.

2.2. Preparation of M-γFS nanocomposite materials

At room temperature, M-γFS was prepared at the optimum conditions according to the evaluation experiments on preparation parameters: 0.8 g γ-Fe_2O_3 was added to a mixture of ethanol and DI water (v/v 80:20) and ultrasonically dispersed for 60 min. After dispersion, 2 mL ammonium was added and homogeneously mixed. A mixture solution of 0.4 mL TEOS and 30 mL ethanol was then added in drops and stirred at 200 r/min for 3 h. The composite materials were washed three times in ethanol and then dried at 60 °C in an oven for 12 h. After cooling, the materials were ground to obtain the orange M-γFS powder.

2.3. Adsorption experiment

An amount of M-γFS powder was added to 50 mL MB with initial concentrations of 15–180 mg/L. The initial solution pH was adjusted to 4.0–12.0 by adding 0.1 M HCl or 0.1 M NaOH, and the solution was then shaken at 150 r/min at temperature 298–318 K for 0.5–6 h. After that, M-γFS was separated from the solution with an external magnetic field, the solution absorbance was measured at 664 nm. All samples were prepared in duplicate, and average values of the replicated measurements were reported in all experiments. The adsorption capacity of MB on M-γFS, q_e (mg/g) was calculated using Eq. (1):

$$q_e = V\frac{C_0 - C_e}{M} \tag{1}$$

Where q_e is the adsorption capacity, C_0 is the initial MB concentration, C_e is the equilibrium MB concentration, V is the volume of the solution and M is the mass of the adsorbents.

2.4. Instrumentation

A glass pH electrode (PHS-25, China) was used for pH measurement. Sample morphology was examined using a transmission electron microscope (TEM, JEM-100CXII, Japan). X-ray diffraction (XRD) were performed on the samples to confirm the crystal structure and identity using X-ray Diffractometer (Rigaku D/MAX-RB, Japan) with Cu Kα radiation in the 2θ ranges of 5°∼80° at a scan rate of 1 °/min. The FTIR spectrum of SiO_2, γ-Fe_2O_3, M-γFS before and after adsorption was measured with NICOLET 5700 FTIR Spectrometer (Thermo Fisher Scientific). The specific surface area was determined with a

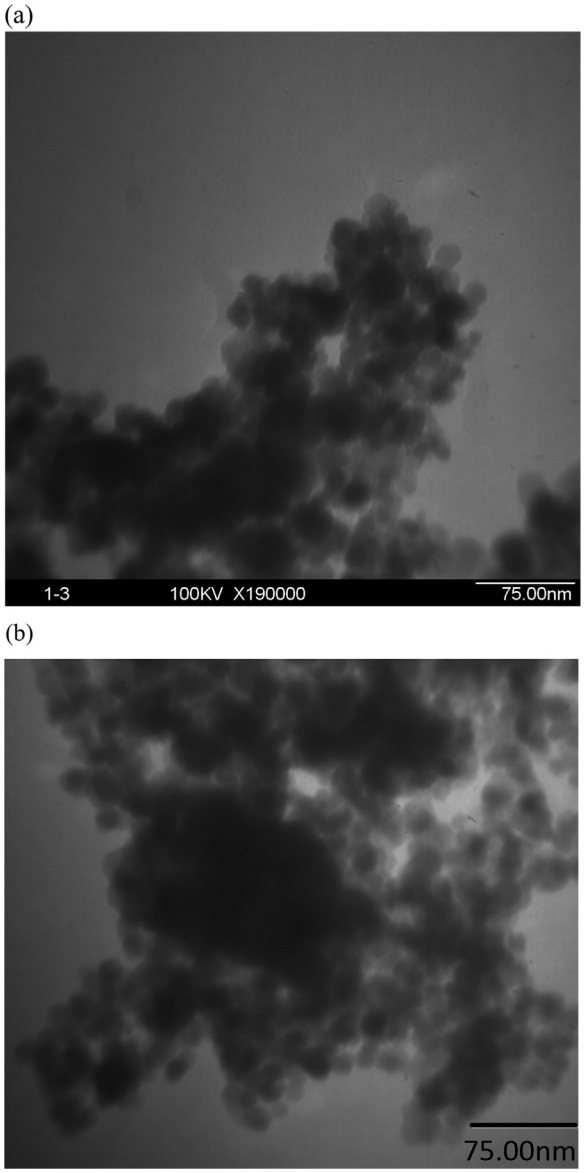

Fig. 1. TEM images of (a) γ-Fe_2O_3 and (b) M-γFS.

specific surface area analyzer (Micromeritics, USA) and calculated by the Brunauer-Emmett-Teller (BET) method. Magnetization measurements were obtained using a vibrating sample magnetometer (LAKESHORE-740, USA) at room temperature. UV–vis detection was carried out on a TU-1950 double beam UV–vis Spectrophotometer (Purkinje General, China). The characterizations of the samples were carried out at their optimal conditions.

3. Results and discussion

3.1. Characterization of materials

3.1.1. TEM image and X-ray diffraction analysis

TEM image of the γ-Fe_2O_3 and M-γFS particles are shown in Fig. 1(a) and (b). Compared with γ-Fe_2O_3 particles in Fig. 1 (a), because M-γFS particles easily aggregated in solution, SiO_2 was coated along the surface of aggregation, and an irregular core-shell structure formed as illustrated in Fig. 1(b). M-γFS particles presents non-uniformity after γ-Fe_2O_3 particles were coated with SiO_2. The average diameter of the γ-Fe_2O_3 is 34 nm and that of the M-γFS nanoparticle is 38 nm, respectively, indicates that the average coating thickness of SiO_2 on the surface of γ-Fe_2O_3 is approximately 2 nm.

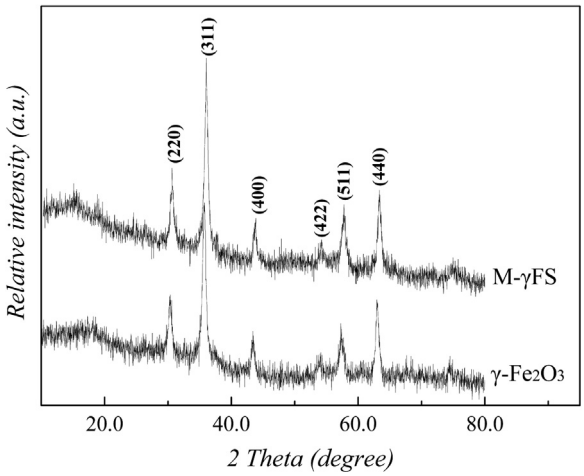

Fig. 2. XRD patterns of γ-Fe_2O_3 and M-γFS.

Fig. 2 displays that the XRD diffraction peaks for M-γFS particle are consistent with that of γ-Fe_2O_3 in the obvious peaks at 2 Theta 30° (220), 44° (400), 57° (511) and 63° (440). Additionally, SiO_2 characteristic peaks appear at 2 Theta 36° (311) and 42° (400), indicating that SiO_2 has been successfully coated on the surface of γ-Fe_2O_3 and does not change the crystal structure of γ-Fe_2O_3.

3.1.2. BET specific surface area, pore size distribution and magnetic saturation intensity

The specific surface area directly governs the contact interfacial area that is available for adsorption. Generally speaking, the adsorption capacity increases with increasing specific surface area. The N_2 adsorption isotherm of M-γFS and pore size distribution are presented in Fig. 3(a) and (b). According to the classification of gas adsorption isotherms (Fig. 3(a)), the

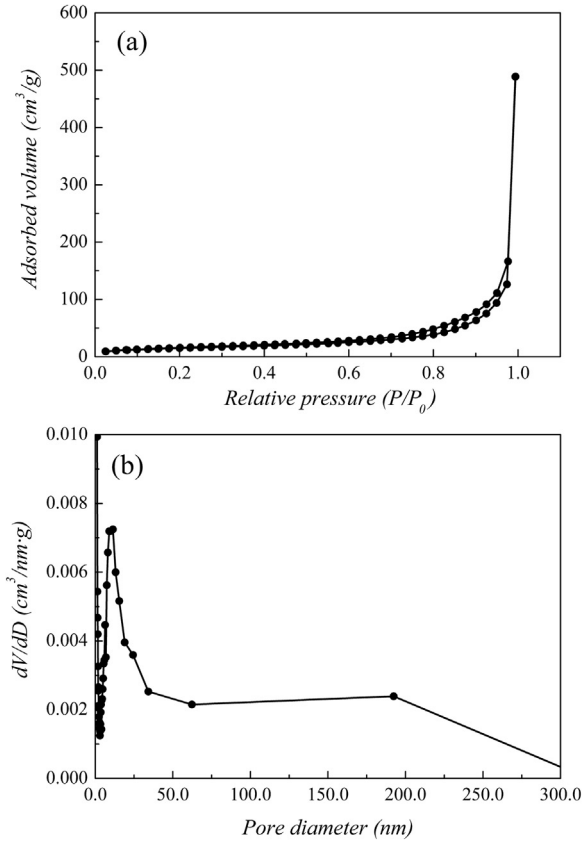

Fig. 3. (a) Adsorption isotherm of N_2 on M-γFS; (b) Pore size distribution of M-γFS.

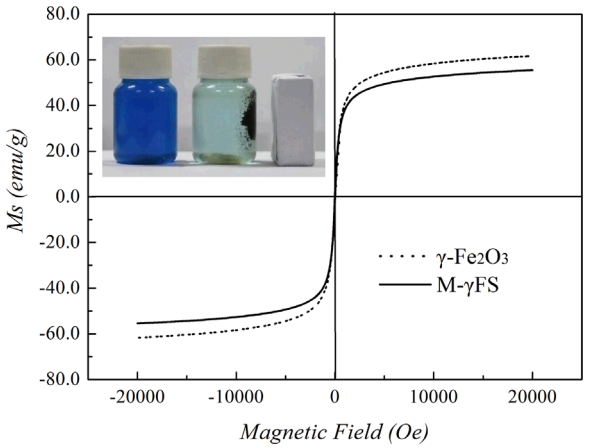

Fig. 4. Hysteresis curves of γ-Fe_2O_3 and M-γFS, and image of separating M-γFS from MB solution by magnetic field.

nitrogen adsorption isotherm of M-γFS exhibits a plateaus line at low pressures, whereas at high pressures, the adsorption isotherm steep straight. The calculated specific surface area of the M-γFS is 74.35 m^2/g, and that of γ-Fe_2O_3 is 68.10 m^2/g which is not illustrated with figure. In the meanwhile, Fig. 3(b) presents most of the pore size distribution of M-γFS is around 10 nm.

Fig. 4 exhibits obviously the hysteresis curves of γ-Fe_2O_3 and M-γFS. From Fig. 4, the γ-Fe_2O_3 particles has 62 emu/g (300 K) of magnetic saturation intensity, whereas M-γFS particles is 55 emu/g (300 K) for it. As a result, the coating of SiO_2 on the surface of M-γFS can increase the specific surface area while decreasing the magnetic saturation intensity of M-γFS. However, the slight decrease of magnetic saturation intensity has not influenced the magnetic separation. Therefore, M-γFS particles can act as strong magnetic carriers in the adsorption process. The picture embedded in Fig. 4 also reveals that the magnetic saturation intensity is strong enough to separate adsorbents from MB solution in a magnetic field.

3.2. Effect of various parameters on the adsorption of MB

3.2.1. Effect of contact time

Herein, firstly we compared the adsorption capacity for MB on different materials SiO_2, γ-Fe_2O_3 and M-γFS. As can be seen from Fig. 5, γ-Fe_2O_3 particles have no adsorption ability for MB, only play as the magnetic carrier role. It is noteworthy that the adsorption capacity for MB on the coated SiO_2 in M-γFS can get to a much high adsorption capacity with 116.09 mg/g. In this study, the quality ratio of γ-Fe_2O_3 to the coated SiO_2 is 8:1 in M-γFS, the adsorption capacity for MB on the coated SiO_2 in M-γFS was calculated by the quality ratio and the adsorption capacity of M-γFS. The ratio of adsorption capacity for MB on M-γFS with 12.8 mg/g to that on the coated SiO_2 is very close to the quality ratio of γ-Fe_2O_3 to coated SiO_2. Therefore, γ-Fe_2O_3 occupies a large portion of composite materials M-γFS only as a magnetic carrier, but it is the coated SiO_2 on the surface of M-γFS that act as the main adsorption function for the dye MB.

It is also clear that the adsorption capacity of the coated SiO_2 in M-γFS is 4.5 times to the solo SiO_2 with 25.3 mg/g (Fig. 5). Particularly, the adsorption of MB on M-γFS only requires 0.5 h to reach adsorption balance, however the solo SiO_2

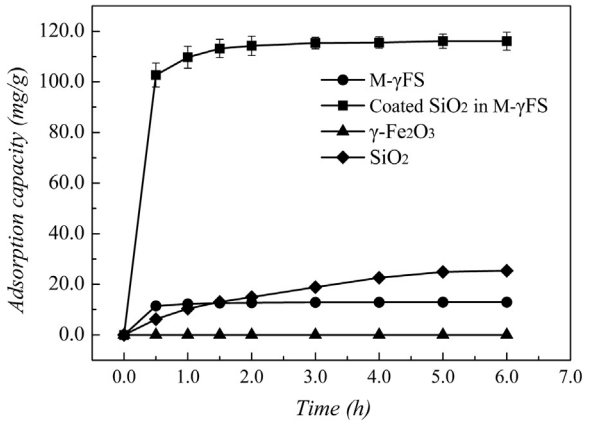

Fig. 5. Effect of contact time for different materials. (initial pH 7.0, temperature 298 K, initial MB concentration 30 mg/L, M-γFS dosage 2 g/L, γ-Fe_2O_3 dosage 2 g/L, SiO_2 dosage 0.22 g/L.).

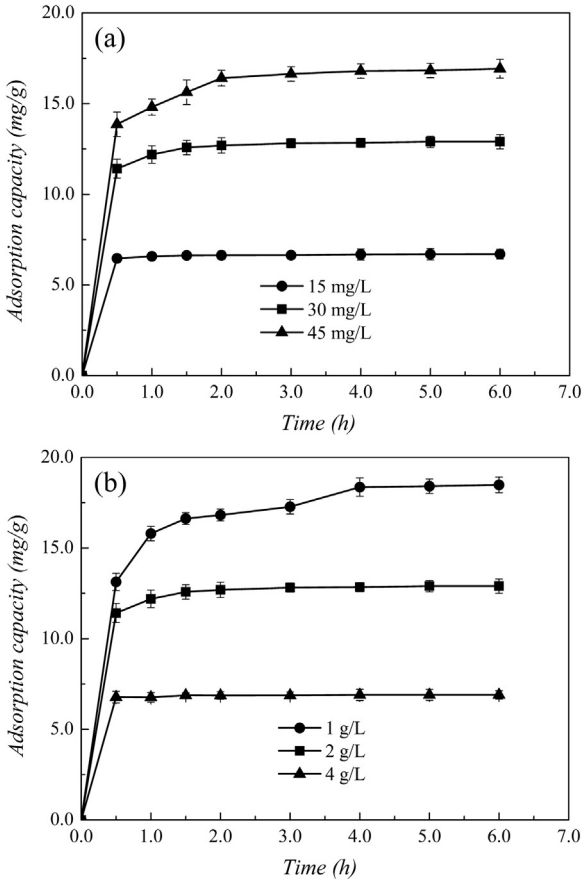

Fig. 6. Effect of contact time for M-γFS. (a) at different initial MB concentrations 15 mg/L, 30 mg/L, 45 mg/L (initial pH 7.0, temperature 298 K, dosage of M-γFS 2 g/L.); (b) at different dosages 1 g/L, 2 g/L, 4 g/L. (initial pH 7.0, temperature 298 K, initial MB concentration 30 mg/L.).

requires 6 h to reach adsorption balance. We could suggest that combination of SiO_2 and γ-Fe_2O_3 can make the surface of nano γ-Fe_2O_3 homogenous, and enhance greatly the contacting area between SiO_2 and contaminants, consequently make the adsorption to be ongoing more adequately and rapidly.

On the other hand, if compared with the maximum adsorption capacity of MB on other adsorbents such as nitric acid-treated bamboo waste with 87.72 mg/g [25], oil palm empty fruit bunch fibers with 68.6 mg/g [26], SnO_2 quantum dots decorated silica nanoparticles with 73.15 mg/g [18], and magnetic responsive metal–organic frameworks nanosphere with 73.8 mg/g [27], the coated SiO_2 in M-γFS not only has performed higher adsorption capacity than these adsorbents but also has a strong separation ability from water assisted by the magnetic field.

In the following experiments and discussion, the adsorption capacity of M-γFS is signified by the total mass of M-γFS. Fig. 6(a) and (b) illustrates the effect of contact time on the adsorption capacity of MB on M-γFS at different initial MB concentration and dosage of M-γFS. These figures show that the adsorption of MB on M-γFS is a fast process, and part equilibrium can be reached after adsorption for 2 h while whole equilibrium can be reached after adsorption for 4 h. In addition, lower initial MB concentrations and larger quantities of M-γFS require shorter time to reach equilibrium. Therefore, when M-γFS is used in dyeing wastewater treatment, the dosage of M-γFS can be appropriately increased to improve the effect of adsorption and shorten adsorption time.

3.2.2. Effect of pH values of initial solution

When discussing the effects of pH values of initial solution on the adsorption process, the effects of pH on MB molecules should be considered. As observed from Fig. 7(a), with different pH values 4.0, 7.0 and 12.0 of initial solution, although the adsorption maximum occurs excursion compared to the initial fixed 664 nm, the excursion and change are very tiny. Therefore, the influence of error is negligible.

Fig. 7(b) shows the effect of pH values of initial solution on adsorption capacity. From Fig. 7(b), the alkaline conditions are beneficial to the adsorption of MB on M-γFS. As we know, MB is a heterocyclic aromatic chemical compound with the chemical formula $C_{16}H_{18}N_3SCl$. Under alkaline conditions, MB tends to form cations, whereas OH^- is adsorbed to the surface of M-γFS to form negatively charged adsorption centers, thus promoting the adsorption of MB ions.

In order to scientifically explore the adsorption mechanism, we compared the changes of zeta potential before and after

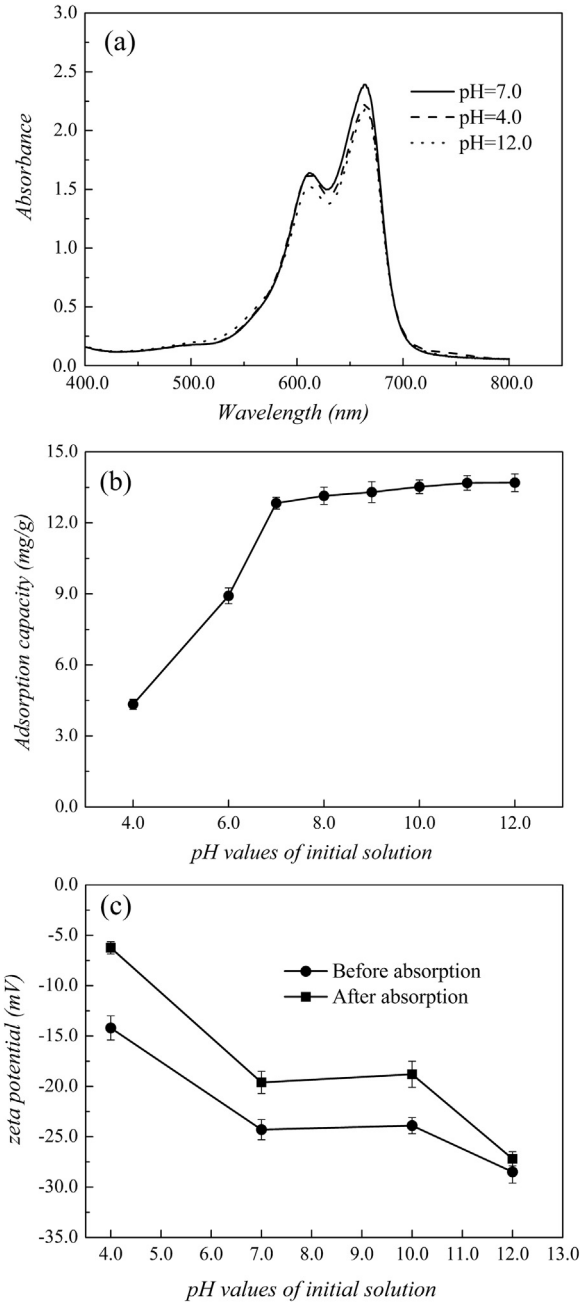

Fig. 7. Effect of pH values of initial solution on (a) absorbance, (b) adsorption capacity and (c) zeta potential. (temperature 298 K, initial MB concentration 30 mg/L, M-γFS dosage 2 g/L, contact time 4 h.).

adsorption of MB. Zeta potential value of M-γFS under different pH values was detected and shown in Fig. 7(c). M-γFS appears to be negative charge in solution, and zeta potential decreases with pH increases, indicating that M-γFS can adsorb OH^- in solution. As discussed above, alkaline conditions can promote the adsorption of MB ions on M-γFS. MB in solution is easy to ionize Cl^- anion in solution, and displays charge positivity. Thereby improve its adsorption onto M-γFS. Similarly, the fact of zeta potential value of M-γFS after adsorption decreasing can also confirm this viewpoint.

3.2.3. *Effect of initial MB concentration*

Fig. 8 displays the effect of different initial MB concentrations on the adsorption capacity at different temperatures. The figure shows that increases of initial MB concentration can enhance the adsorption of MB onto M-γFS. An increase in the initial MB concentration can improve the force driving MB from the solution to the surface of M-γFS, thus causing the movement of equilibrium towards adsorption. It was found that the adsorption arrived saturation when the initial MB

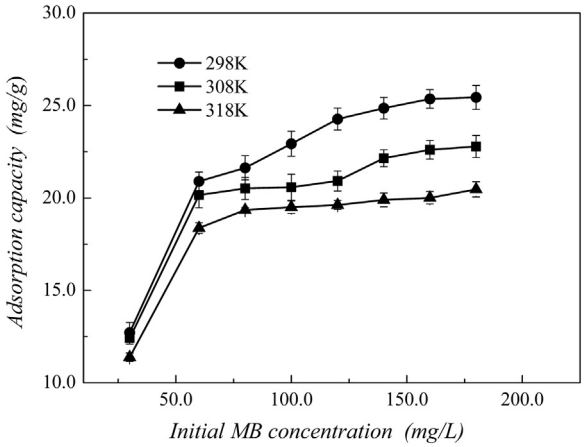

Fig. 8. Effect of initial MB concentration. (initial solution pH 7.0, temperature 298 K, 308 K and 318 K, M-γFS dosage 2 g/L, contact time 4 h.).

concentration is 180 mg/L, and the adsorption capacity is 25.4 mg/g, 22.8 mg/g, and 20.5 mg/g at 298 K, 308 K, and 318 K, respectively.

3.2.4. *Effect of coexisting cations, ionic strength and humic acid*

Fig. 9(a)–(c) shows the effects of coexisting cations, ionic strength and humic acid in the solution on the adsorption capacity. Fig. 9(a) illustrates that the coexisting cations in solution can decrease the adsorption of MB on M-γFS, and the ions with the order of weak to strong influences are Ca^{2+}, Cu^{2+}, and Cr^{3+}. We could explain the results by these reasons. On the one hand, M-γFS exhibits adsorption ability for cations by reducing the adsorption sites on the surface while repelling MB with a positive charge. Meanwhile, the cations with larger radii and higher charges can decrease the adsorption more significantly. On the other hand, there may be a cation complexation interaction between Ca^{2+}, Cu^{2+}, or Cr^{3+}, and MB molecules. The competitive adsorption among metallic cations and MB cations on M-γFS can also be considered one of the reasons to decrease the adsorption capacity.

Fig. 9(b) shows that high ionic strength can dramatically decrease the adsorption capacity of MB, attributing to the fact that the increase of ionic strength can cause the salt to screen the electrostatic interactions between adsorbents and dyes, consequently resulting in the decrease of dye adsorption. However, with a subsequent increase in the sodium chloride concentration, the ionic strength increases and the adsorption capacity can be recovered, due to a double layer structure could be formed because of electrostatic interactions when the solid and liquid come into contact. In addition, an increase of ionic strength can make the positive and negative ions rise in solution, and thus neutralize partially adsorption sites on the adsorbents. Accordingly, the double layer is compressed, and the dye molecules are able to more easily approach to the surface of the adsorbents and thus to increase the interactions.

Fig. 9(c) displays that humic acid at low concentration of 0–2 g/L can promote the adsorption of MB on M-γFS, whereas excess humic acid reduces the adsorption performance. As a natural polymer, humic acid exhibits excellent adsorption and chelation with heavy metal ions and dyes in water [28]. Humic acid at low concentrations may attach to the surface of M-γFS particles and support the adsorption of MB. However, the excess humic acid not only occupies a lot of adsorption sites on the surface of M-γFS and obstructs the passageway among particles, but also it can decrease the solution pH values, which are not beneficial for the adsorption process.

3.3. *Adsorption kinetics*

In this study, two different kinetic models were used: (1) the pseudo-second order kinetic model (Eq. (2)) and (2) the intraparticle diffusion model (Eq. (3)) [29–31]:

The pseudo-second order kinetic could be shown by Eq. (2):

$$\frac{t}{q_t} = \frac{1}{k_2 q_e^2} + \frac{1}{q_e} t \tag{2}$$

Where q_e is the amount sorbed at equilibrium (mg/g), k_2 is the equilibrium rate constant of pseudo-second order (g/mg h). These constants can be determined by plotting t/q_t against t.

The intraparticle diffusion kinetic (Weber-Morris diffusion model) is shown in Eq. (3) [32]:

$$q_t = k_{id} t^{1/2} + C \tag{3}$$

Where K_{id} (g/mg h) is the rate constant of the interaparticle diffusion kinetic model. The value of C and K_{id} is obtained from

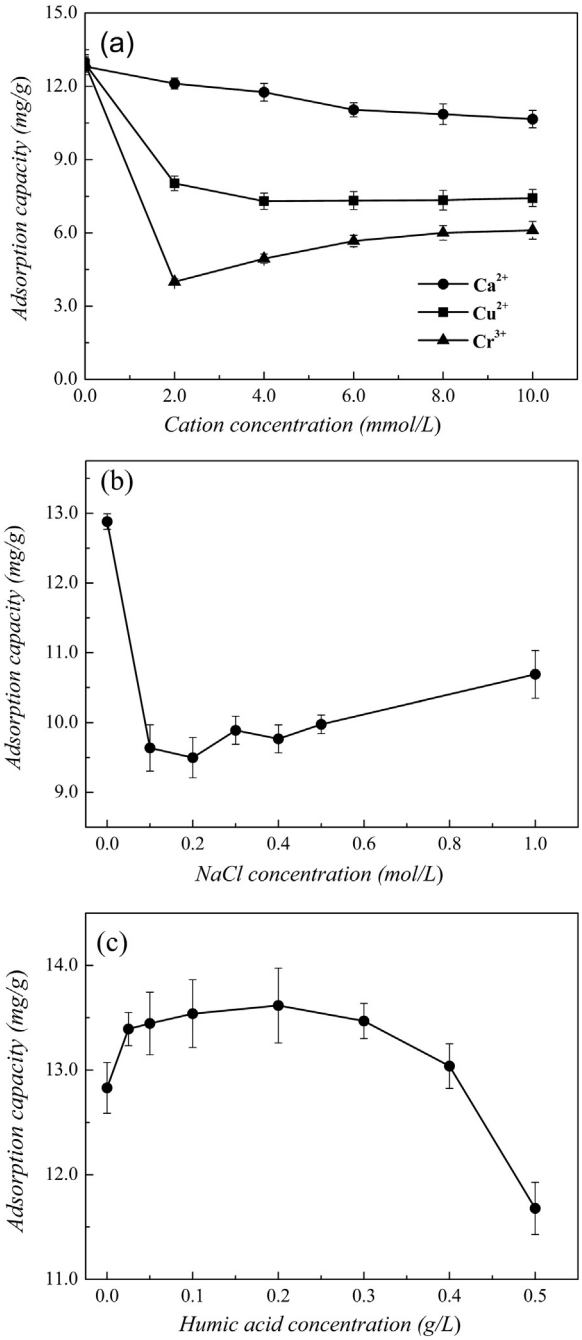

Fig. 9. Effect of (a) coexisting cations, (b) ionic strength and (c) humic acid. (initial pH 7.0, temperature 298 K, initial MB concentration 30 mg/L, M-γFS dosage 2 g/L, contact time 4 h.).

the intercept and slope of the line plotted in q_t against $t^{1/2}$, respectively.

As presented in Table 1, Graphs 1(a), 1(b) and Graphs 2(a), 2(b) in supplementary materials, the adsorption kinetics data of M-γFS is accordance with the pseudo-second-order kinetics model, but inconsistent with the intraparticle diffusion model. Lines with the intraparticle diffusion model did not pass through the origin, indicating the intraparticle diffusion is not the only speed-controlled step for the adsorption.

3.4. Adsorption isotherm

In order to understand and clarify the adsorption process, Langmuir, Freundlich and Dubinin-Radushkevich (D-R)

Table 1
Kinetics parameters of pseudo-second-order and intraparticle diffusion model for MB adsorption on M-γFS.

Parameters	$q_{e\ (exp)}$ (mg/g)	Pseudo-second-order			Intraparticle diffusion model		
		$q_{e\ (cal)}$ (mg/g)	k_2 (g/mg h)	R^2	c (mg/g)	k_{id} (mg/g h)	R^2
C_0 (mg/L)							
15	6.698	6.720	6.221	1	2.740	2.365	0.464
30	12.899	13.051	1.210	1	4.794	4.759	0.541
45	16.927	17.343	0.408	0.999	5.539	6.465	0.626
M (g/L)							
1	18.483	19.264	0.207	0.999	5.170	7.278	0.708
2	12.899	13.051	1.121	1	4.794	4.759	0.541
4	6.897	6.916	9.910	1	2.861	2.428	0.454

isotherm models are applied in this study [33,34]. Langmuir isotherm is assumed that adsorption is a monolayer adsorption and the maximum adsorption occurs when molecules adsorbed on the surface of sorbent form a saturated layer. The Langmuir equation is

$$\frac{c_e}{q_e} = \frac{1}{K_L q_m} + \frac{c_e}{q_m} \tag{4}$$

Where q_e is the amount sorbed at equilibrium (mg/g), C_e is the equilibrium concentration (mg/L), q_m is the maximum adsorption capacity (mg/g), and K_L is the adsorption intensity or Langmuir coefficient related to the affinity of the binding site (L/mg).

The Freundlich isotherm can be applied to non-ideal adsorption on heterogeneous surfaces as well as multilayer adsorption and is expressed by Eq. (5):

$$\ln q_e = \ln K_F + \frac{1}{n} \ln c_e \tag{5}$$

Where K_F and $1/n$ is the constants that are related to the adsorption capacity and the adsorption intensity, respectively.

The D-R equation is used to explain energetic heterogeneity of solid surface at the monolayer region in micro-pores, and the equation may be represented as:

$$\ln q_e = \ln q_m - \beta\varepsilon^2 \tag{6}$$

Where q_e is the amount of adsorbate per unit weight of sorbent (mol/g), q_m is the D-R monolayer adsorption capacity (mol/g), β is a constant related to adsorption energy (mol^2/kJ^2), and ε is the Polanyi potential, which is equal to

$$\varepsilon = RT \ln(1 + 1/c_e) \tag{7}$$

Adsorption energy E (kJ/mol), can be obtained by Eq. (8):

$$E = (2\beta)^{-1/2} \tag{8}$$

It means energy for per mol sorbate in transfer from infinity in solution to the surface.

Table 2 and Graph 3(a)–3(c) in supplementary materials demonstrate that compared with the Freundlich and D-R isotherm models, the Langmuir equation is more suitable for describing the adsorption behavior of MB on M-γFS. According to the hypothesis of the Langmuir model, MB was adsorbed on the surface of M-γFS as a monolayer, and the adsorption is uniformly distributed to all adsorption sites.

The value of the average activation energy (E) can be used to explain the adsorption mechanism [35]: when |E| is less than 8 KJ/mol, physical adsorption plays *a* dominant role; and when |E| is 8–16 KJ/mol, chemical ion exchange plays *a* dominant role. The |E| value calculated from the D-R model is 0.302–0.434 KJ/mol, indicating that the adsorption of MB on M-γFS is mainly physical adsorption. When the temperature increases, the q_m value decreases, and it suggests the MB

Table 2
The parameters of Langmuir, Freundlich and D-R isotherms at different temperatures.

T (K)	Langmuir			Freundlich			D-R		
	q_m (mg/g)	K_L (L/mg)	R^2	n	K_F	R^2	q_m (mg/g)	R^2	E (kJ/mol)
298	26.617	0.154	0.999	5.068	10.322	0.901	23.934	0.917	0.434
308	23.419	0.182	0.997	6.023	10.507	0.816	21.582	0.954	0.414
318	20.956	0.215	0.999	5.749	9.194	0.752	19.882	0.993	0.302

Table 3
Thermodynamic parameters for MB adsorption on M-γFS.

T (K)	lnKc	ΔG (kJ/mol)	ΔH (kJ/mol)	ΔS (J/ (mol · K))	R^2
298	1.02	−2.53	−22.33	−66.05	0.84
308	0.87	−2.24			
318	0.45	−1.20			

adsorption on M-γFS is an exothermic process.

3.5. Adsorption thermodynamics

The adsorption free energy (ΔG°), standard enthalpy (ΔH°) and standard entropy (ΔS°) are calculated from the adsorption of MB on M-γFS at different temperatures [36]. Based on thermodynamic theory, the relationship is shown as the following Eqs. (9–11), respectively:

$$\Delta G = \Delta H - T\Delta S \tag{9}$$

$$K_c = \frac{q_e}{c_e} \tag{10}$$

$$\ln K_c = -\frac{\Delta H}{RT} + \frac{\Delta S}{R} \tag{11}$$

Where R is the gas constant (8.314 J/mol K) and T is the absolute temperature (K). Thus, ΔH° and ΔS° are obtained from the slope and intercept of the line plotted by $\ln(Q_e/C_e)$ versus $1/T$, respectively.

The enthalpy change (ΔH) and entropy change (ΔS) can be obtained according to the 1/T plotted against lnKc. The slope and intercept obtained from the fitted line was used to calculate the thermodynamic parameters shown in Table 3. These parameters show that the ΔG values are negative for the experimental temperatures, demonstrating that the adsorption of MB on M-γFS is a spontaneous process. More negative values of ΔG can promote an easier adsorption process. The ΔH values are negative, suggesting that the adsorption of MB on M-γFS is an exothermic process, and this result is consistent with previous results. The ΔS values are negative, revealing that the ordered arrangement at the solid-liquid interface increases in the adsorption process.

3.6. FTIR spectra of M-γFS before and after adsorption

Fig. 10 figures out the FTIR spectra of SiO_2, γ-Fe_2O_3, and M-γFS before and after adsorption. It is obvious that the characteristic adsorption peaks in wavenumber 446 cm^{-1}, 555 cm^{-1}, 637 cm^{-1} and 696 cm^{-1} belong to Fe–O bond in γ-Fe_2O_3. Strong adsorption peaks wavenumber in 1071 $cm^{-1}$and 798 cm^{-1} are Si–O bond. Meanwhile, these peaks can be observed in the FTIR spectra of M-γFS, which further confirm that SiO_2 have been successfully coated on the surface of γ-Fe_2O_3. The peaks at M-γFS have not changed after MB adsorption, suggesting that M-γFS has a strong ability in steady which is advantageous for cyclic utilization.

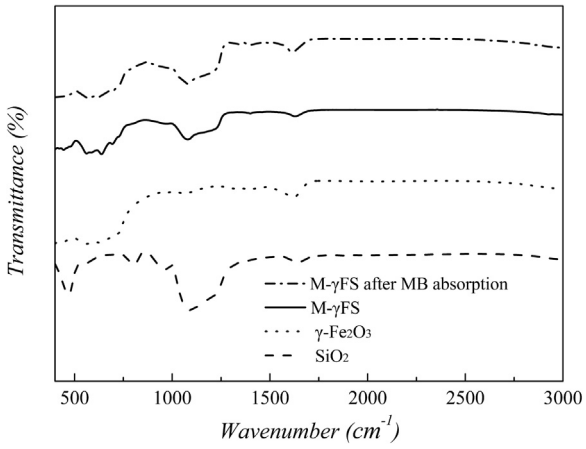

Fig. 10. FTIR spectra of SiO_2, γ-Fe_2O_3, M-γFS before and after adsorption.

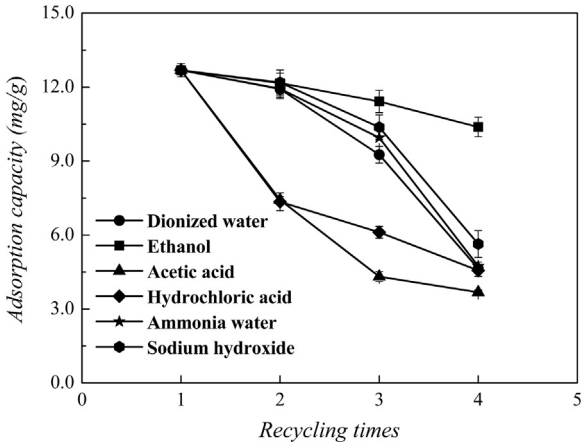

Fig. 11. Effect of recycling times on adsorption capacity using different solvents.

3.7. Regeneration of M-γFS

The regeneration process was carried out under the conditions: initial MB concentration 30 mg/L, M-γFS dosage 2 g/L, initial solution pH 7.0, temperature 298 K, and contact time 4 h. Afterward, the used M-γFS were washed with DI water and other five solvents of ethanol (EtOH), acetic acid (AC), hydrochloric acid (HCl), ammonium water (AW) and NaOH solution in the concentration of 1 mol/L, and then were dried for reuse. The results of the regeneration in Fig. 11 reveal that ethanol can achieve a highest recovery for the adsorption capacity of M-γFS in all solvents. M-γFS can still keep 10.39 mg/g of adsorption capacity and 80% removal of MB by ethanol solvent after M-γFS recycled four times.

4. Conclusions

The M-γFS exhibits an irregular core-shell structure with average diameter of the particles 38 nm, the specific surface area 74.35 m^2/g, and the magnetic saturation intensity 55 emu/g. The optimum adsorption of MB on M-γFS occurred in alkaline conditions, and the maximum adsorption capacity calculated by coated SiO_2 in M-γFS is 116.09 mg/g. Coexisting cations and ionic strength can decrease the adsorption performance of M-γFS, whereas humic acid at low concentration can promote the adsorption of MB on M-γFS.

The adsorption of MB on M-γFS shows a good fit to the pseudo-second-order kinetics model, and intraparticle diffusion is not the only speed-controlled step. The Langmuir isotherm is more suitable for describing the adsorption behavior of MB on M-γFS, and the results suggest that the adsorption is a spontaneous process. In addition, the ordered arrangement at the solid-liquid interface can be increased during the adsorption process.

Meanwhile, M-γFS can still keep 80% removals of MB by ethanol-washed and recycling four times. Moreover, due to low cost, eco-friendly, non-toxicity and high adsorption capacity of M-γFS, the magnetic adsorbent can be considered as one of the effective options to remove MB from dye wastewater.

Acknowledgements

The support from the planning project on innovation and entrepreneurship training of China is gratefully acknowledged.

Appendix A. Supplementary material

Supplementary data associated with this article can be found in the online version at http://dx.doi.org/10.1016/j.wri.2016.05.003.

References

[1] M. Vakili, M. Rafatullah, B. Salamatinia, A.Z. Abdullah, M.H. Ibrahim, K.B. Tan, Z. Gholami, P. Amouzgar, Application of chitosan and its derivatives as adsorbents for aye removal from water and wastewater: a review, Carbohydr. Polym. 113 (2014) 115–130.
[2] J. Fu, G.Z. Kyzas, Wet air oxidation for the decolorization of dye wastewater: an overview of the last two decades, Chin. J. Catal. 35 (2014) 1–7.

[3] H. Zangeneh, A.A.L. Zinatizadeh, M. Habibi, M. Akia, M. Hasnain Isa, Photocatalytic oxidation of organic dyes and pollutants in wastewater using different modified titanium dioxides: a comparative review, J. Ind. Eng. Chem. 26 (2015) 1–36.
[4] E. Alver, A.Ü. Metin, Anionic dye removal from aqueous solutions using modified zeolite: adsorption kinetics and isotherm studies, Chem. Eng. J. 200 (2012) 59–67.
[5] J.Z. Guo, B. Li, L. Liu, K. Lv, Removal of methylene blue from aqueous solutions by chemically modified bamboo, Chemosphere 111 (2014) 225–231.
[6] B. Li, Y.L. Feng, J.Z. Guo, L.Q. Bai, J. Chen, L. Liu, L.Q. Zhang, Amorphous coordination polymer with high adsorption ability for anionic dyes from aqueous solution, Sci. Adv. Mater. 5 (2013) 341–345.
[7] S.Z. Ajabshir, M.S. Niasari, M. Hamadanian, Praseodymium oxide nanostructures: novel solvent-less preparation, characterization and investigation of their optical and photocatalytic properties, RSC Adv. 5 (2015) 33792–33800.
[8] S. Moshtaghi, S.Z. Ajabshir, M.S. Niasari, Nanocrystalline barium stannate: facile morphology-controlled preparation, characterization and investigation of optical and photocatalytic properties, J. Mater. Sci.: Mater. Electron. 27 (2016) 834–842.
[9] S.Z. Ajabshir, M.S. Niasari, M. Hamadanian, Preparation of nanocrystalline praseodymium oxide with different shapes via a simple thermal decomposition route, J. Mater. Sci.: Mater. Electron. 27 (2016) 998–1006.
[10] F. Beshkar, S.Z. Ajabshir, M.S. Niasari, Preparation and characterization of the $CuCr_2O_4$ nanostructures via a new simple route, J. Mater. Sci.: Mater. Electron. 26 (2015) 5043–5051.
[11] S.M. Derazkola, S.Z. Ajabshir, M.S. Niasari, Novel simple solvent-less preparation, characterization and degradation of the cationic dye over holmium oxide ceramic nanostructures, Ceram. Int. 41 (2015) 9593–9601.
[12] N. Ren, X. Zhou, W. Guo, S. Yang, A review on treatment methods of dye wastewater, CIESS J. 64 (2013) 84–94. (Chinese journal).
[13] P. Sivakumar, P.N. Palanisamy, Adsorption studies of basic red 29 by a nonconventional activated carbon prepared from Euphorbia antiquorum L, J. Chem. Tech. Res. 1 (2009) 502–510.
[14] L. Zhou, J. Chen, F. Yu, Z. Yuan, J. Ma, Adsorption of methylene blue on magnetic multiwalled carbon nanotube synthesized by Fenton reaction, Environ. Chem. 31 (2012) 669–675. (Chinese journal).
[15] Y. Liu, M. Zhou, H. Tang, J. Miao, S. Zhu, Absorption of methylene blue on sludge activated carbon, Chin. J. Environ. Eng. 6 (2012) 2339–2344. (Chinese journal).
[16] Y. Houndonougbo, C. Signer, N. He, W. Morris, H. Furukawa, K.G. Ray, D.L. Olmsted, M. Asta, B.B. Laird, O.M. Yaghi, A combined experimental-computational investigation of methane adsorption and selectivity in a series of isoreticular zeolitic imidazolate frameworks, J. Phys. Chem. C 117 (2013) 10326–10335.
[17] Ö. Şahin, M. Kaya, C. Saka, Plasma-surface modification on bentonite clay to improve the performance of adsorption of methylene blue, Appl. Clay Sci. 116–117 (2015) 46–53.
[18] D. Dutta, D. Thakur, D. Bahadur, SnO_2 quantum dots decorated silica nanoparticles for fast removal of cationic dye (methylene blue) from wastewater, Chem. Eng. J. 281 (2015) 482–490.
[19] M. Wawrzkiewicz, M. Wiśniewska, V.M. Gun'ko, V.I. Zarko, Adsorptive removal of acid, reactive and direct dyes from aqueous solutions and wastewater using mixed silica-alumina oxide, Powder Technol. 278 (2015) 306–315.
[20] D. Wei, B. Wang, H.H. Ngo, W. Guo, F. Han, X. Wang, B. Du, Q. Wei, Role of extracellular polymeric substances in biosorption of dye wastewater using aerobic granular sludge, Bioresour. Technol. 185 (2015) 14–20.
[21] Z. Wu, H. Zhong, X. Yuan, H. Wang, L. Wang, X. Chen, G. Zeng, Y. Wu, Adsorptive removal of methylene blue by rhamnolipid-functionalized graphene oxide from wastewater, Water Res. 67 (2014) 330–344.
[22] S.L. Lin, Z.L. Song, G.B. Che, A. Ren, P. Li, C.B. Liu, J.S. Zhang, Adsorption behavior of metal-organic frameworks for methylene blue from aqueous solution, Microporous Mesoporous Mater. 193 (2014) 27–34.
[23] H.Y. Zhu, R. Jiang, L. Xiao, W. Li, A novel magnetically separable γ-fe2o3/crosslinked chitosan adsorbent: preparation, characterization and adsorption application for removal of hazardous azo dye, J. Hazard Mater. 179 (2010) 251–257.
[24] A. Ahmadi, S. Heidarzadeh, A.R. Mokhtari, E. Darezereshki, H.A. Harouni, Optimization of heavy metal removal from aqueous solutions by maghemite (γ-Fe_2O_3) nanoparticles using response surface methodology, J. Geochem. Explor. 147 (2014) 151–158.
[25] B.H. Hameed, I.A.W. Tan, Nitric acid-treated bamboo waste as low-cost adsorbent for removal of cationic dye from aqueous solution, Desalination Water Treat. 21 (2010) 357–363.
[26] M.S. Sajab, C.H. Chia, S. Zakaria, P.S. Khiew, Cationic and anionic modifications of oil palm empty fruit bunch fibers for the removal of dyes from aqueous solutions, Bioresour. Technol. 128 (2013) 571–577.
[27] Y. Shao, L. Zhou, C. Bao, J. Ma, M. Liu, F. Wang, Magnetic responsive metal–organic frameworks nanosphere with core–shell structure for highly efficient removal of methylene blue, Chem. Eng. J. 283 (2016) 1127–1136.
[28] X. Xu, D. Xu, H. Chu, Removal of reactive brilliant red from wastewater using lignite humic acid, J. Saf. Environ. 11 (2011) 62–65. (Chinese journal).
[29] C. Namasivayam, M.V. Sureshkumar, Removal of chromium (vi) from water and wastewater using surfactant modified coconut coir pith as a biosorbent, Bioresour. Technol. 99 (7) (2008) 2218–2225.
[30] G. Du, Z. Lia, L. Liao, R. Hanson, S. Leick, N. Hoeppner, W.T. Jiang, Cr (VI) retention and transport through Fe (III)-coated natural zeolite, J. Hazard Mater. 221 (2012) 118–123.
[31] H. Nourmoradi, M. Nikaeen, M. Khiadani, Removal of Benzene, Toluene, Ethylbenzene and Xylene (BTEX) from aqueous solutions by montmorillonite modified with nonionic surfactant: equilibrium, kinetic and thermodynamic study, Chem. Eng. J. 191 (2012) 341–348.
[32] W.J. Weber, J.C. Morris, Kinetics of adsorption on carbon from solution, J. Sanit. Eng. Div. Am. Soc. Civ. Eng. 89 (1963) 31–60.
[33] A. Nilchi, T.S. Dehaghan, S.R. Garmarodi, Kinetics, Isotherm and thermodynamics for uranium and thorium ions adsorption from aqueous solutions by crystalline tin oxide nanoparticles, Desalination 321 (2013) 67–71.
[34] V. Ranjithkumar, S. Sangeetha, S. Vairam, Synthesis of magnetic activated carbon/α-Fe_2O_3 nanocomposite and its application in the removal of acid yellow 17 dye from water, J. Hazard Mater. 273 (2014) 127–135.
[35] S.D. Yusan, S.A. Erenturk, Sorption behaviors of uranium (VI) ions on α-FeOOH, Desalination 269 (1) (2011) 58–66.
[36] M. Al-Ghouti, M.A.M. Khraisheh, M.N.M. Ahmad, S. Allen, Thermodynamic behaviour and the effect of temperature on the removal of dyes from aqueous solution using modified diatomite: A kinetic study, J. Colloid Interface Sci. 287 (2005) 6–13.